

## MICROCHANNEL PLATE DETECTORS ✓

JOSEPH LADISLAS WIZA

*Galileo Electro-Optics Corporation, Sturbridge, Massachusetts, U.S.A.*

### 1. Introduction

A microchannel plate (MCP) is an array of  $10^4$ – $10^7$  miniature electron multipliers oriented parallel to one another (fig. 1); typical channel diameters are in the range 10–100  $\mu\text{m}$  and have length to diameter ratios ( $\alpha$ ) between 40 and 100. Channel axes are typically normal to, or biased at a small angle ( $\sim 8^\circ$ ) to the MCP input surface. The channel matrix is usually fabricated from a lead glass, treated in such a way as to optimize the secondary emission characteristics of each channel and to render the channel walls semiconducting so as to allow charge replenishment from an external voltage source. Thus each channel can be considered to be a continuous dynode structure which acts as its own dynode resistor chain. Parallel electrical contact to each channel is provided by the deposition of a metallic coating, usually Nichrome or Inconel, on the front and rear surfaces of the MCP, which then serve as input and output electrodes, respectively. The total resistance between electrodes is on the order of  $10^9 \Omega$ . Such microchannel plates, used singly or in cascade, allow electron multiplication factors of  $10^4$ – $10^7$  coupled with ultra-high time resolution ( $< 100$  ps) and spa-

tial resolution limited only by the channel dimensions and spacings; 12  $\mu\text{m}$  diameter channels with 15  $\mu\text{m}$  center-to-center spacings are typical.

Originally developed as an amplification element for image intensification devices, MCPs have direct sensitivity to charged particles and energetic photons which has extended their usefulness to such diverse fields as X-ray<sup>1)</sup> and E.U.V.<sup>2)</sup> astronomy, e-beam fusion studies<sup>3)</sup> and of course, nuclear science, where to date most applications have capitalized on the superior MCP time resolution characteristics<sup>4–6)</sup>.

The MCP is the result of a fortuitous convergence of technologies. The continuous dynode electron multiplier was suggested by Farnsworth<sup>7)</sup> in 1930. Actual implementation, however, was delayed until the 1960s when experimental work by Oschepkov et al.<sup>8)</sup> from the USSR, Goodrich and Wiley<sup>9)</sup> at the Bendix Research Laboratories in the USA, and Adams and Manley<sup>10–11)</sup> at the Mullard Research Laboratories in the U.K. was described in the scientific literature. These developments relied heavily on a wealth of information on secondary electron emission<sup>12)</sup> and earlier work on the technique of producing resistive surfaces in lead glasses by high temperature reduction (250–450  $^\circ\text{C}$ ) in a hydrogen atmosphere<sup>13)</sup>. Finally, since most of the electrical performance characteristics of channel multipliers are not a function of channel length,  $l$ , or channel diameter,  $d$ , separately, but only a function of the ratio  $l/d = \alpha$ , an almost arbitrary size reduction is possible. Such size reduction may be achieved by glass fiber drawing techniques which form the basis of fiber optic device fabrication<sup>14)</sup>. In addition to a significant dimensional reduction resulting from these methods, a logarithmic compression of repetitive manufacturing steps is also possible, i.e., one can achieve a structure with  $\sim 10^6$  holes requiring  $\sim 2 \times 10^3$  fiber alignment steps by a draw/multi-draw technique.

Prior to the application of reliable fiber drawing techniques, however, the first operational MCPs

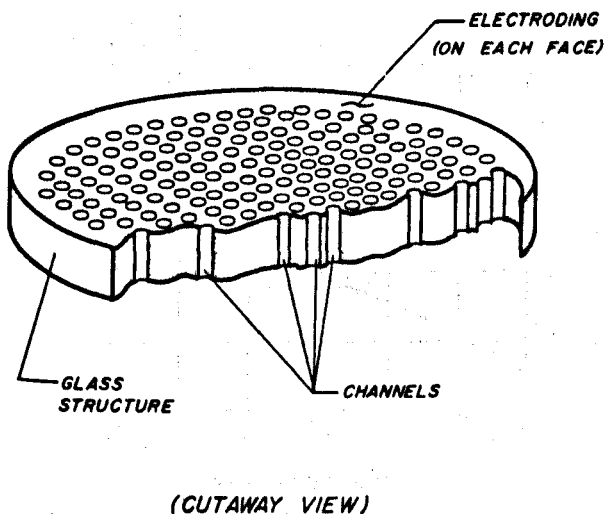


Fig. 1. A microchannel plate.

were built between 1959 and 1961 at Bendix Research Laboratories<sup>15</sup>). The first models were assembled from thousands of single channel electron multipliers ( $\sim 150 \mu\text{m}$  channel spacing) by bonding them together with a low melting point solder or frit glass.

## 2. Theory of operation

The theory of channel multiplication has been adequately covered by many authors<sup>11,16-17</sup>). The aim here is to present results from a simple theoretical analysis which pertain to particular MCP design parameters. We shall consider here the phenomena of ion feedback, space charge saturation, and dimensional scaling. Recently, a computer model has been developed<sup>18</sup>) which uses Monte Carlo methods to predict the performance of straight channel multipliers. It is well to keep in mind that predictions based on this model are in much closer agreement with experimental data than those of the simple theory considered here.

### 2.1. THE STRAIGHT CHANNEL ELECTRON MULTIPLIER

A diagram of a straight channel electron multiplier is shown in fig. 2. Pictured here is a simple mechanism where an incident electron produces  $\delta$  secondary electrons. The kinematics are such that  $\delta^2$  secondary electrons are produced in the second stage,  $\delta^3$  in the third, etc., so that the overall gain  $G$  is given by  $G = \delta^n$ . According to Schagen<sup>17</sup>), assuming that the secondary emission is normal to the channel walls,

$$G = \left( \frac{AV}{2\alpha V_0^{1/2}} \right)^{4V_0\alpha^2/V}, \quad (1)$$

where

$V$  is the total channel voltage,

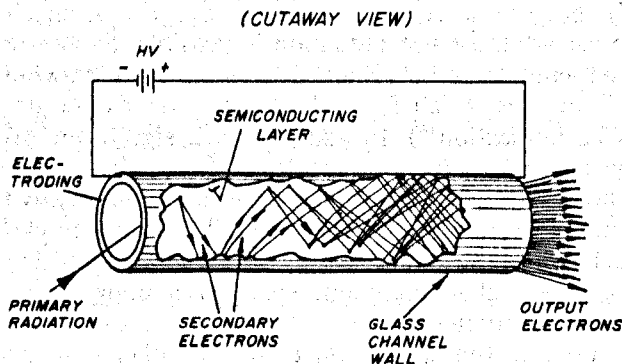


Fig. 2. A straight channel electron multiplier.

$V_0$  is the initial energy of an emitted secondary electron  $\sim 1 \text{ eV}$ ,  $\alpha$  is the length to diameter ratio, and  $A$  is the proportionality constant in the assumed relation

$$\delta = AV_c^{1/2}, \quad (2)$$

where  $V_c$  is the electron collision energy in eV, and  $A \sim 0.2$ . As  $V$  increases, so does  $\delta$ , the secondary electron yield, since each collision then occurs at a higher energy  $V_c$ . At the same time, the number of collisions within the channel must decrease, resulting in an extremum in the  $G$  vs  $V$  characteristic. A measured characteristic curve is shown in fig. 3 for a Galileo MCP with straight channels. Rather than exhibiting a maximum, the curve levels off at large  $V$ ; this is due to secondary emission which is not orthogonal to the channel walls. We note here that the computer model of Guest<sup>18</sup>) does show good agreement with experimental data.

Eq. (1) also exhibits an extremum in  $\alpha$ , suggesting that there is a gain for which the inevitable variations in  $\alpha$  from channel to channel have minimal effect. From eq. (1) and the condition  $d(\ln G)/d\alpha = 0$ , we find that

$$\alpha_M = \frac{AV}{3.3 V_0^{1/2}} = \frac{V}{16.5}, \quad (3)$$

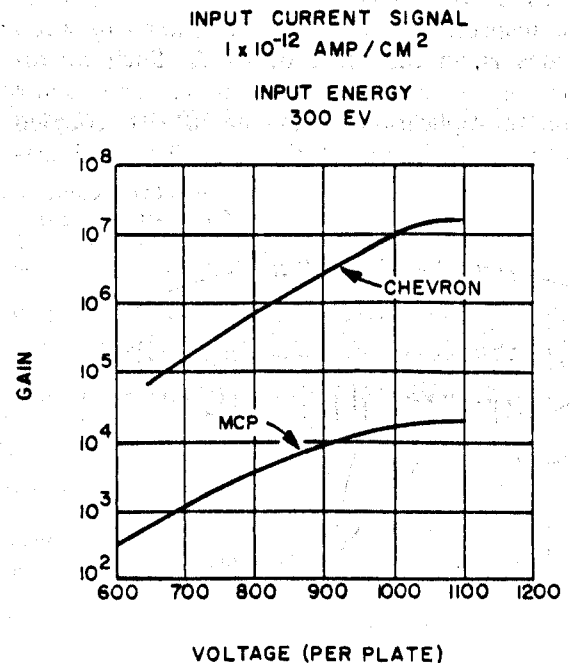


Fig. 3. Gain vs voltage characteristic for a straight channel MCP and a Chevron.

and

$$G_M = \exp(0.184 A^2 V) = \exp(0.0074 V), \quad (4)$$

where  $G_M$  and  $\alpha_M$  are the values of  $G$  and  $\alpha$  at the extremum. For  $V=1$  kV,  $G_M=1635$  and  $\alpha_M=60$ . According to Guest<sup>18</sup>),  $\alpha_M = V/22$  so that  $\alpha_M=45$ . In any event,  $\alpha$  is typically in the range 40–60 for MCPs used in image intensification.

The statistics of the channel multiplication process are such that the charge pulse height distribution from an MCP with straight channels approximates a negative exponential. Such a distribution obtained in the author's laboratory is shown in fig. 4. This data was obtained by single electron excitation of a Galileo MCP. Output electrons were post-accelerated into a fast phosphor, and the resulting light pulses observed with a photomultiplier tube. Finally, the analysis of Guest<sup>18</sup>) indicates that the energy distribution of electrons emerging from a straight channel is a quasi-negative exponential. For example, with  $\alpha=60$  and  $V=1000$  V, the exiting electrons have a median energy of 32.5 eV and an appreciable number have energies in excess of 100 eV.

Straight channel multipliers typically operate at gains of  $10^3$ – $10^5$ , the upper limit being set by the onset of ion feedback and the resulting performance instabilities. As the gain increases, so does the probability of producing positive ions in the

high charge density region at the output of the channel. These ions are produced by electron collisions with residual gas molecules at ambient pressures greater than  $10^{-6}$  torr and with gas molecules desorbed from the channel walls under electron bombardment. Such ions can drift back to the channel input, producing ion after pulses. In the case of a vacuum tube with a proximity focus photocathode, these ions can produce additional secondary electrons at the photocathode, resulting in a regenerative feedback situation.

In case of large single channels, ion feedback can be suppressed simply by bending<sup>19–20</sup>) or twisting<sup>21</sup>) the channels.

## 2.2. THE CURVED CHANNEL ELECTRON MULTIPLIER, SPACE CHARGE SATURATION

As the suppression of ion feedback allowed operation of single channel multipliers at higher gains, it was found that the charge pulse height distribution changed radically from a negative exponential to a quasi-Gaussian shape with a full width at half maximum (fwhm) of 50% or better at a peak gain of  $10^8$  or more. Such behavior is the result of space charge saturation near the channel output<sup>20</sup>). At high enough gains, the space charge density at the rear of the channel reduces the kinetic energy of electrons as they interact with the channel walls until the secondary electron yield  $\delta$  is reduced to unity. This then is a state of dynamic equilibrium, i.e., for a decrease in space charge density the electron kinetic energy at collision increases and so does  $\delta$  and consequently, the space charge density; conversely, if the space charge density increases, the collisional energy decreases so that  $\delta$  drops to less than unity, producing a corresponding reduction in the space charge density. Thus, the channel gain is limited by the space charge density which itself is defined by the channel geometry and the overall channel voltage. Schmidt and Hendee<sup>20</sup>) and more recently, Loty<sup>22</sup>) have shown that the maximum gain from a space charge saturated channel, for a fixed  $V$  and  $\alpha$ , is proportional to the channel diameter. Therefore, since a 1 mm diameter channel saturates at a gain of  $10^8$ , a 10  $\mu$ m diameter channel should saturate at  $10^6$ . This suggests that microchannel plates ( $\sim 25$   $\mu$ m pore size), suitably engineered to suppress ion feedback should exhibit saturated gains in the low  $10^6$  range, which has indeed been found to be the case<sup>23,24</sup>).

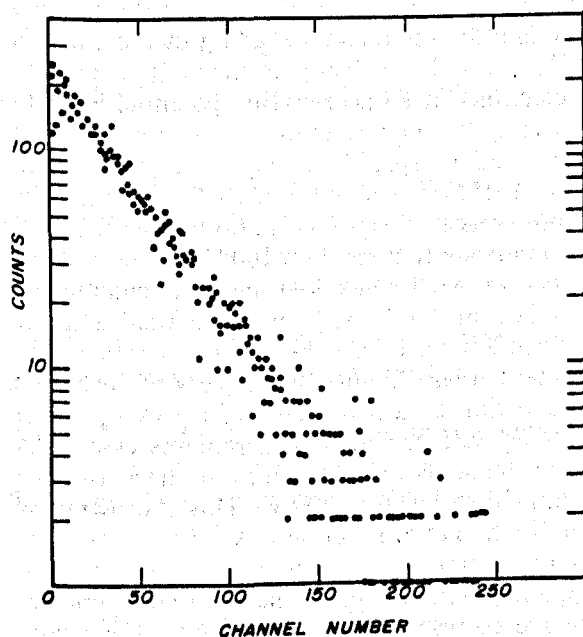


Fig. 4. Pulse amplitude distribution from a straight channel MCP.

The phenomenon of space charge saturation and the resulting quasi-Gaussian pulse height distribution allows an integral discriminator to be set for event counting so that the measured count rates are relatively insensitive to gain shifts. In other words, the count rate vs. bias voltage characteristic exhibits a reasonably flat plateau; the latter cannot be obtained with a negative exponential charge distribution.

### 2.2.1. The Chevron

As noted above, ion feedback suppression may be achieved in single channel multipliers by the simple expedient of curving the channel. Such a device is difficult to achieve in a thin ( $\sim 0.5$  mm) microchannel plate and a commonly used method of obtaining high gain space charge saturated output pulses is the MCP Chevron described by Col-

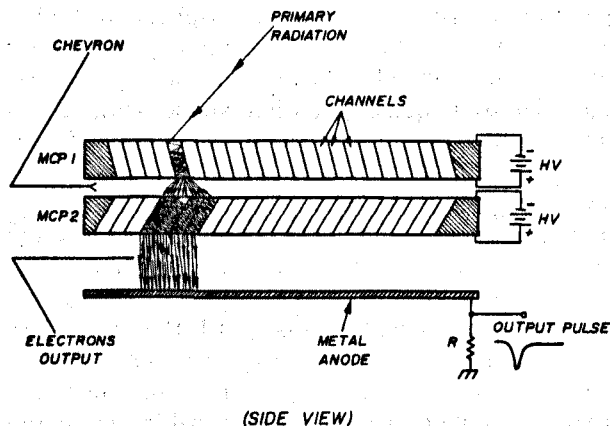


Fig. 5. Chevron operation.

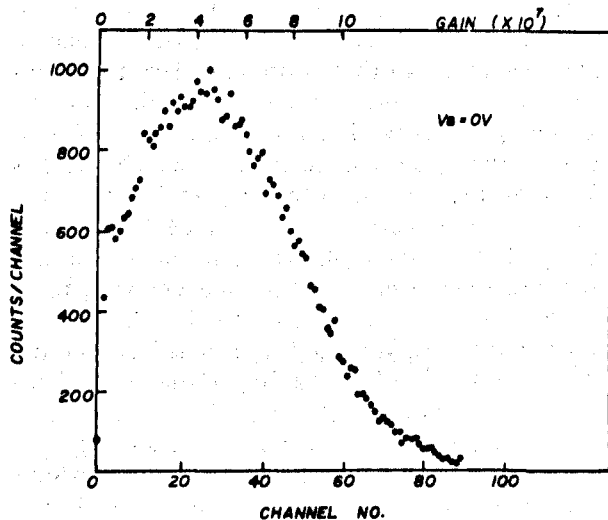


Fig. 6. Chevron pulse amplitude distribution at 1 kV/plate.

son et al.<sup>26</sup>) and which is shown schematically in fig. 5. The plates are oriented so that the channel bias angles (typically  $8^\circ/8^\circ$  or  $0^\circ/15^\circ$ ) provide a sufficiently large directional change so as to inhibit positive ions produced at the output of the rear plate from reaching the input of the front plate. A gain vs. voltage curve for a Chevron is shown in fig. 3. Typically the plates are separated by  $50\text{--}150\text{ }\mu\text{m}$  and individually operated at gains in the  $10^4$  range. A pulse height spectrum obtained with low energy positive ion bombardment of a Galileo Chevron is shown in fig. 6. The MCPs were 25 mm in diameter and had  $12\text{ }\mu\text{m}$  diameter channels ( $\alpha \sim 40$ ) biased at an angle of  $8^\circ$  to the input surface normal. The bias voltage was 1 kV per plate, and the plate separation was  $150\text{ }\mu\text{m}$ . The output electrons were accelerated by 270 V to a collecting plate and the resulting charge pulses were analyzed using standard NIM electronics. The peak gain is high ( $\sim 4 \times 10^7$ ) and the distribution quite broad (fwhm  $\sim 170\%$ ). For a  $50\text{ }\mu\text{m}$  plate separation, the peak gain is typically  $(1\text{--}2) \times 10^7$  with a fwhm of  $120\text{--}150\%$ .

We have recently investigated the effect of interplate bias voltage,  $V_B$ , on the output pulse height distribution<sup>27</sup>). Referring to fig. 5, the charge distribution from MCP 1 is exponential with a mean gain of  $\sim 10^4$  and a mean electron energy of 30 eV. At such low charge densities, space charge effects are negligible and the primary mechanism for interplate spreading of the electron cloud is the radial velocity component of the exiting electrons. If an accelerating potential is applied between the plates, there is less time for the charge cloud to spread radially, and fewer channels in MCP 2 are excited, but each is driven harder into space charge saturation. Our calculations<sup>27</sup>) indicate that for  $V_B = 100$  V, the number of channels in MCP 2 excited by one channel in MCP 1 is reduced by slightly more than a factor 3. Such reasoning is in substantial agreement with experiment. Figs. 7a and 7b are plots of peak gain,  $G_p$ , and fwhm as a percentage of  $G_p$  vs  $V_B$ . After an initial falloff, the peak gain remains essentially constant while fwhm continues to decrease, approaching 60% at  $V_B = 700$  V. This narrowing of the pulse height distribution is advantageous in many pulse processing schemes, since the dynamic range requirements on subsequent electronic circuitry are correspondingly diminished. For example, amplitude dependent discriminator walk is reduced.

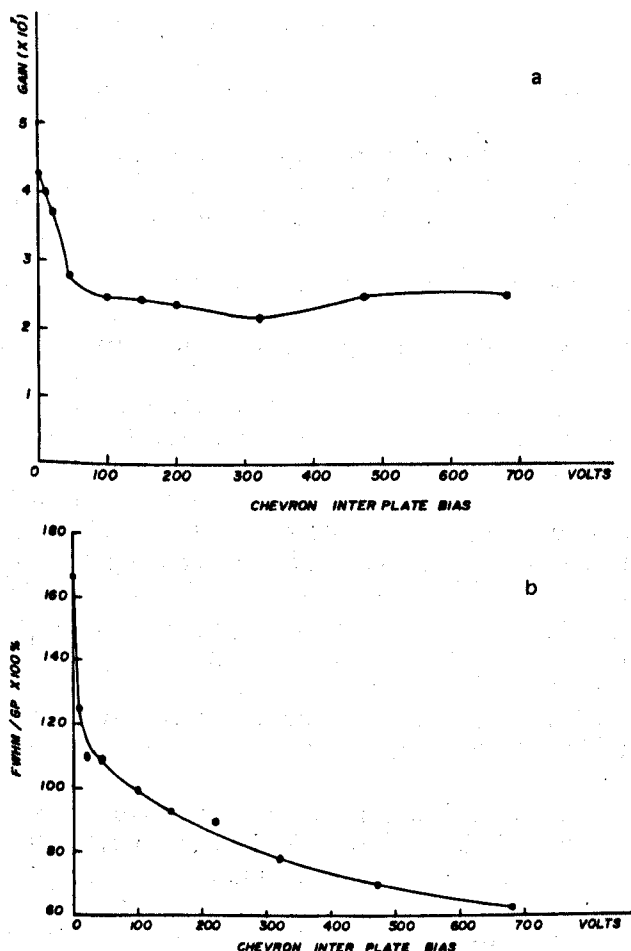


Fig. 7. (a) Gain vs interplate bias voltage for a Chevron at 150  $\mu\text{m}$  plate separation. (b) Normalized full width at half-maximum ( $\text{fwhm}/G_p \times 100\%$ ) vs Chevron interplate bias voltage.

The Chevron therefore exhibits high saturated gains ( $>10^7$ ) because of the multiplicity of channels excited in MCP 2 by a single channel in MCP 1. In imaging applications where the output electron distribution is mapped onto a phosphor screen for direct viewing, or a multi-anode array, the Chevron does exhibit a degradation in spatial resolution because of this interplate charge spreading. However, where spatial information is obtained by centroid averaging methods, such as the resistive anode with either charge division or rise time encoding, spatial resolution down to a single channel dimension in MCP 1 has been observed<sup>28</sup>).

### 2.2.2. The curved channel MCP

The first microchannel plates having curved channels were described in 1974 by Boutot et al.<sup>29</sup>)

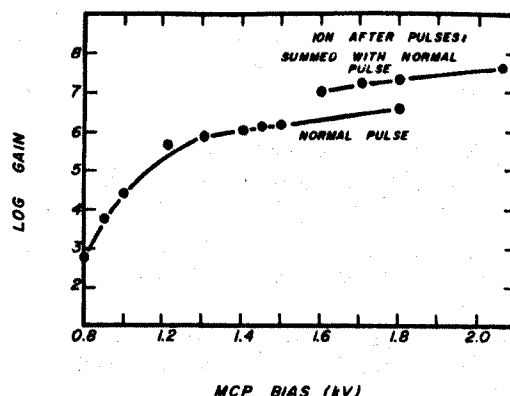


Fig. 8. Gain vs voltage characteristic for a Galileo high gain curved channel plate.

from LEP<sup>30</sup>) and preliminary results with Mulard<sup>31</sup>) curved channel MCPs were recently described by Timothy<sup>32,33</sup>). Plate diameters were typically 25 mm with channel diameters in the range 12–40  $\mu\text{m}$  and  $\alpha=80$ . Saturated gains were in the low  $10^6$  range, as might be expected, based on the scaling of single channel gains to these smaller dimensions. Typical fwhm values for the saturated pulse height distributions were in the 60% range.

Curved channel MCPs manufactured by Galileo Electro-Optics Corp. were recently described by Henkel et al.<sup>24</sup>). The plates were 25 mm in diameter with 25  $\mu\text{m}$  curved channels ( $\alpha=70$ ). A gain vs. voltage characteristic curve is shown in fig. 8, which also shows the contribution of ion feedback. Below  $5 \times 10^5$  gain (1300 V) there is no evidence of ion feedback and the Gaussian pulse amplitude distribution is narrow ( $\text{fwhm} \sim 60\%$ ). Tests on later versions of this plate indicate feedback-free operation at gains of  $(2-3) \times 10^6$  (1350 V).

### 2.2.3. Other high gain configurations

Other approaches to achieving saturated pulse height distributions free of ion feedback have been reported in the literature. In 1974, Timothy<sup>32</sup>) described a plate which employed an angled electrostatic field to inhibit ion feedback. This technique relied on the presence of insulating strips inserted in the wall of each microchannel to establish the angled electrostatic field. The output pulse height distribution was indeed saturated at high gain, but unfortunately, charging of the insulating strips cause a time dependent reduction in gain. Consequently, such plates are really only useful at very low count rates.

A rather interesting configuration is the Chev-

ron with interposed mesh described by Henkel et al.<sup>24</sup>). A metal mesh having square holes  $44\text{ }\mu\text{m}$  on a side was placed between the MCPs ( $12\text{ }\mu\text{m}$  channels,  $\alpha = 40$ ) of a standard Chevron operated with 1000 V across the front and 700 V across the rear plate. The gain was comparable to that of a conventional Chevron ( $\sim 2 \times 10^7$ ) but the saturated pulse amplitude distribution had a fwhm of only 50%. The thickness of the mesh was  $75\text{ }\mu\text{m}$ . Other metal meshes were used and broader pulse height distributions resulted, suggesting a critical relationship between channel diameter, mesh opening, and spacing. The mesh presumably restricts the charge spreading between plates, having an effect similar to that obtained with an interplate bias voltage.

### 3. Manufacturing technology

The technology of MCP manufacture was reviewed by Washington et al.<sup>14</sup>) in 1971 and only a brief description of the method most familiar to the author, i.e., the etchable core technique employed at Galileo Electro-Optics, will be presented here.

The basic steps used to obtain the unprocessed MCP wafer are shown in fig. 9. Single channels are drawn as solid-glass fibers having two components, a core glass, soluble in a chemical etchant, and a lead glass cladding which is not soluble in the core glass etchant, and which will eventually form the MCP matrix structure. The fibers from the first draw are packed together in a hexagonal

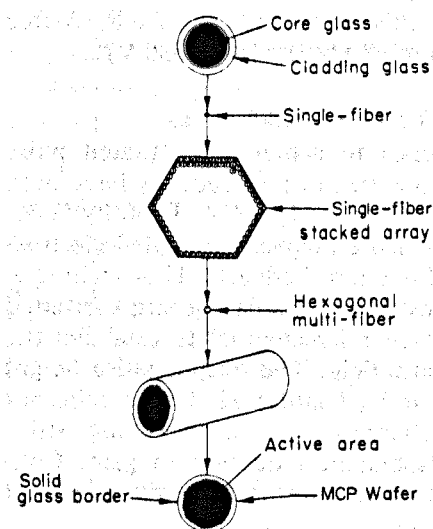


Fig. 9. Etchable core MCP manufacturing process.

array, and drawn again into hexagonal multi-fibers. The latter are stacked again and fused within a glass envelope to form a boule. This boule is then sliced, often at a small angle ( $8^\circ$ - $15^\circ$ ) from the normal to the channel axes; the resulting wafers are then edged, beveled and polished into a thin plate. The soluble core glass is then removed by a suitable chemical etchant, and after some additional chemical processing to enhance the secondary electron emission characteristics of the channel walls, the plates are reduced in a hydrogen furnace.

The lead oxide at the glass surface is converted to semiconducting lead and water. The lead particles, however, tend to agglomerate, which prevents them from participating effectively in the electron conduction process<sup>34</sup>). Indeed, when the temperature is too high, the agglomeration process predominates over the formation of new semiconducting lead, resulting in a minimum in the resistivity vs. temperature characteristic, which usually occurs in the  $250$ - $450^\circ\text{C}$  temperature range. Microchannel glass usually develops surface resistivities on the order of  $10^{13}\text{ }\Omega/\square$  so that a typical resistance between electrodes of  $10^9\text{ }\Omega$  is measured. The reduced lead surface has a negative temperature coefficient so that if the resistivity is too low, a thermal runaway condition may occur, resulting in a catastrophic failure of the MCP.

After activation, Inconel electrodes are vacuum deposited on the polished faces of each plate; controlled penetration of electrode material into the output of each channel provides some focusing of the exiting electrons when used with a close proximity phosphor screen.

SEM photographs of a small portion of an MCP before and after processing are shown in fig. 10. The polishing streaks readily visible in the core material are due to the hardness of the core glass in comparison to the lead glass matrix. Also note the high degree of dimensional uniformity from channel to channel, which of course is inherent to the fiber drawing process.

### 4. Performance characteristics

Considered here are those performance characteristics which recommend and also limit the use of MCPs in nuclear science applications, viz. detection efficiency, speed of response, dead time, count rate characteristics, and lifetime.

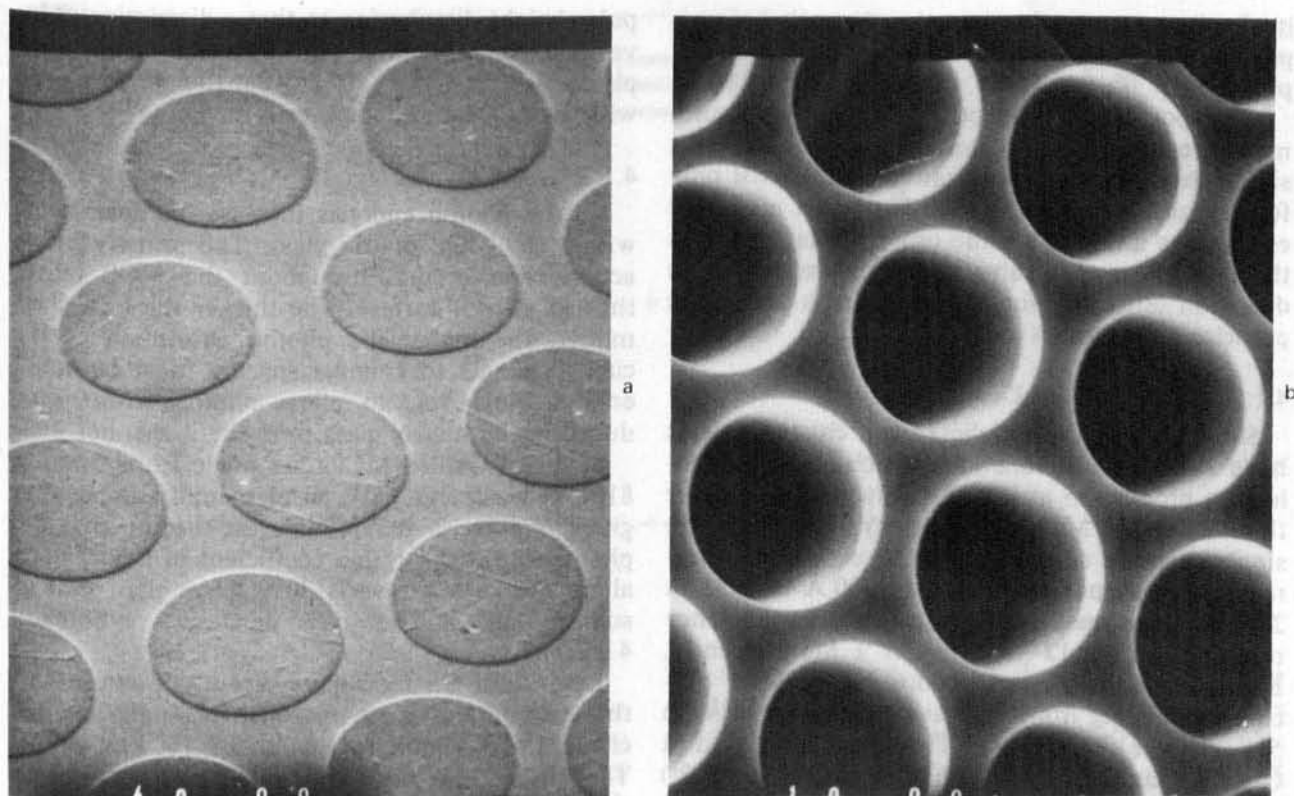


Fig. 10. SEM photographs of an MCP. (a) Before processing. (b) After processing.

#### 4.1. DETECTION EFFICIENCY

The detection efficiency of channel multipliers to various kinds of primary radiation is summarized in table 1 from Schagen<sup>17)</sup> and includes data from single channel multipliers and MCPs. Measurements made with the former are easier to interpret since single channels are usually operated in space charge saturation, allowing the use of pulse counting techniques. More recently, a review of single channel and MCP detection efficiencies has been published by Macau et al.<sup>35)</sup>

##### 4.1.1. Charged particles

The secondary electron emission coefficient,  $\delta$ , for lead glasses typically used in channel plates reaches a maximum of about 2 at an incident primary electron energy of 300 eV<sup>36)</sup>. At low energies, where the incident electrons do not have a range sufficient for multi-channel excitation, the detection efficiency should approach the open area ratio of the MCP which is typically 50%. However, electrons striking the interstitial electrode material produce secondaries which can excite neighboring channels. Galanti et al.<sup>37)</sup> have ob-

served the channel plate efficiency to increase from 50% at 50 eV to 70% at 1 keV. These authors also see a variation of efficiency with the electron angle of incidence, and have reported a maximum at 20° for 1 keV incident electrons. Clearly, if the electron trajectories are almost parallel to the channel axes, there is a high probab-

TABLE 1  
Detection efficiency of channel multipliers<sup>a</sup>.

Type of radiation		Detection efficiency (%)
Electrons	0.2 – 2 keV	50–85
	2 – 50 keV	10–60
Positive ions (H <sup>+</sup> , He <sup>+</sup> , A <sup>+</sup> )	0.5 – 2 keV	5–85
	2 – 50 keV	60–85
	50 – 200 keV	4–60
U.V. radiation	300 – 1100 Å	5–15
	1100 – 1500 Å	1– 5
Soft X-rays	2 – 50 Å	5–15
Diagnostic X-rays	0.12– 0.2 Å	~1

<sup>a</sup> From Schagen<sup>17)</sup>.



ity for deep penetration into the channels before a primary interaction; this results in low gain output pulses near  $0^\circ$ .

Most positive ion detection efficiency measurements reported in the literature have been with single channels, and quantitative results exist only for energies less than 30 keV. However, measured efficiencies are of the same order of magnitude as those for electrons. Tatry et al.<sup>38)</sup> have found the detection efficiency for 40 keV protons and alpha particles to be about 80%.

#### 4.1.2. U.V. and soft X-rays

Single channel multipliers and channel plates have surface work functions which allow photoelectron production at incident wavelengths shorter than 2000 Å. Measurements by Paresce<sup>39)</sup> on single channels suggest an almost exponential decrease in efficiency from 2% at 1200 Å to  $10^{-9}$  at 2600 Å. Other measurements suggest an efficiency near 10% in the 12–70 Å region<sup>40)</sup>. More recently, Bjorkholm et al.<sup>41)</sup> have reported peak MCP efficiencies ranging from 27% at 0.86 keV ( $\sim 14$  Å) to 5% at 3 keV ( $\sim 4.1$  Å). These authors used a Chevron configuration with bias angles of  $(0/8^\circ)$  and  $\alpha = 80$ . They found that the quantum efficiency increases as the angle of incidence decreases until a critical angle is reached after which there is a rapid fall off of efficiency. The peak occurs in the  $1^\circ$ – $6^\circ$  range, and the small angle dip is due to reflection down the channel. They explained the energy variation of quantum efficiency by the variation of the X-ray absorption coefficient, and of the photo and Auger electron ranges; their model assumed a 100 Å layer of  $\text{SiO}_2$  over the lead glass matrix, which is in agreement with the MCP surface analysis studies of Siddiqui<sup>42)</sup>.

Quantum efficiency enhancement can be obtained by vacuum deposition of various high yield photocathode materials on the input face of an MCP. Henry et al.<sup>43)</sup> report an increase of 65% in the quantum efficiency at 1.48 keV using a  $\text{MgF}_2$ -coated plate. The efficiency of electron multipliers with Au, LiF,  $\text{MgF}_2$ , BeO,  $\text{SrF}_2$ , KCl and CsI photocathodes in the 23.6–113 Å wavelength range has been measured by Lukirskii et al.<sup>44)</sup>; CsI is often used at longer wavelengths.

Finally, it should be noted that the use of  $\alpha = 80$  Chevrons for photon detection ensures space charge saturation at small angles of incidence; grazing incidence reflections down the channels for  $\alpha = 40$  plates degrade the resulting

pulse height distribution so that a discriminator level becomes difficult to set. The use of an interplate bias voltage<sup>27)</sup> improves the performance with  $\alpha = 40$  plates, however.

#### 4.1.3. Hard X-rays

As the photon energies increase, so does range within the MCP matrix glass. The primary interaction then occurs throughout the MCP rather than at a front surface. The thicker the lead glass matrix, the higher the photon absorption coefficient; channel to channel spacing must be small enough, however, to allow photoelectrons produced in the matrix glass to excite a channel wall.

Standard Galileo MCPs are made from Corning 8161<sup>45)</sup> glass and have an elemental composition given in table 2. It is of interest to note that the photoelectron absorption coefficient of this material for 662 keV X-rays is 30% larger than that of sodium iodide. The glass density is nominally  $4.0 \text{ g/cm}^3$ .

Dolan and Chang<sup>3)</sup> have recently studied both the current and pulse response of single Galileo channel plates to X-rays in the 8–100 keV range. They found the detection efficiency to vary from 1% to 26%. A plot of efficiency data, taken from ref. 3 is shown in fig. 11. Included here are data obtained by Parkes et al.<sup>46)</sup> and Adams and Millar<sup>47)</sup>. Note that these data were obtained with different channel sizes and angles of incidence; the channel plates were not operated in space charge saturation. Nevertheless, it is apparent that MCPs have a relatively constant efficiency in the 10–600 keV energy range, which makes them somewhat unique in comparison to other X-ray detectors.

TABLE 2  
Elemental composition of MCP glass<sup>a</sup>.

Z	Element	Weight percent
82	Pb	47.8
8	O	25.8
14	Si	18.2
19	K	4.2
37	Rb	1.8
56	Ba	1.3
33	As	0.4
55	Cs	0.2
11	Na	0.1

<sup>a</sup> Density –  $4.0 \text{ g/cm}^3$ .



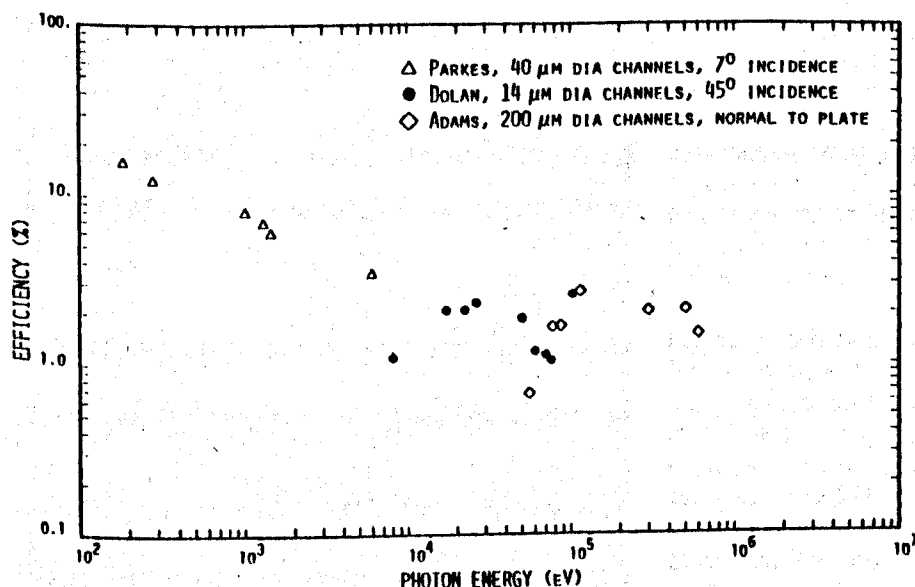


Fig. 11. X-ray detection efficiencies from ref. 3.

#### 4.2. DEAD TIME

The number of channels in a 25 mm diameter MCP with 25  $\mu\text{m}$  diameter channels is about  $5.5 \times 10^5$ . The total plate resistance, electrode to electrode, is typically  $3 \times 10^8 \Omega$ , so that each channel has an associated resistance of  $R_c = 2.75 \times 10^{14} \Omega$ .

If one considers this MCP to be a parallel plate capacitor, 1 mm thick, with half the volume between electrodes filled with Corning 8161 glass (Dielectric constant  $\epsilon = 8.3$ ), then the total plate capacitance is about 200 pF or  $3.7 \times 10^{-16} \text{ F}$  per channel. After a channel "fires" the charge in the channel walls must be replenished, and because of the exponential nature of channel multiplication, most of the charge is depleted from the last 20% of channel length. This means that an effective channel capacitance  $C_c = 7.4 \times 10^{-17} \text{ F}$ , must be recharged through a channel resistance  $R_c = 2.75 \times 10^{14} \Omega$ , so that the recharge time constant, or channel recovery time,  $T_c$ , is given by  $R_c C_c \sim 20 \text{ ms}$ . In general, this kind of analysis predicts that

$$T_c = R_c C_c = Kd, \quad (5)$$

where  $K$  is a proportionality constant which depends on the open area ratio of the MCP and the glass dielectric constant and is on the order of  $4 \times 10^{-13}$  for Galileo plates made from Corning 8161 glass. The linear relation between recovery time and channel diameter for a given resistivity

was discussed by Loty<sup>22</sup>); a dead time of 8 ms for a channel plate with 100  $\mu\text{m}$  diameter pores was determined by Seko and Kobayashi<sup>48</sup>).

Although each channel of an MCP has a dead time on the order of  $10^{-2} \text{ s}$ , the fact that there are  $\sim 10^5$ – $10^6$  channels in a plate which operate more or less independently makes the effective dead time of an MCP on the order of  $10^{-7}$ – $10^{-8} \text{ s}$ , provided no single channel is excited more frequently than once every  $10^{-2} \text{ s}$ , i.e., the incident flux is uniformly distributed over the active area. Measurements in the author's laboratory indicate no serious gain degradation of a uniformly illuminated 25 mm diameter Chevron with 12  $\mu\text{m}$  diameter channels at random count rates up to  $2 \times 10^6 \text{ Hz}$ , in substantial agreement with the above analysis.

When operating a channel plate as a dc current amplifier, the gain is constant until the output current exceeds about 10% of the strip current through the plate; a typical 25 mm plate has a strip current of several  $\mu\text{A}$  at an applied voltage of 1 kV. Loty<sup>22</sup>) has observed that in pulsed operation the peak output current may exceed this conduction current by several orders of magnitude, provided that the repetition rate is sufficiently low, i.e., with period longer than the channel recovery time of several milliseconds.

#### 4.3. TIME OF RESPONSE

The transit time, or the time from initial exci-

tation to the attainment of a given current level at the output of a channel multiplier is a linear function of channel length; space charge saturation produces a degree of standardization in the output pulse amplitudes, so that transit time becomes a well-defined quantity. The resolution with which the time of initial excitation can be measured is determined by the transit time "jitter" which is proportional to the transit time for a given applied voltage and  $1/d$  ratio.

Schmidt and Hendee<sup>20</sup>) found that the saturated pulse width from single channels was proportional to channel length for a given value of  $V/\alpha$ , the normalized field strength. Single channels, 1 mm in diameter with  $\alpha \sim 100$ , produce pulses having a 20–30 ns fwhm. Channel plates (12  $\mu\text{m}$  diameter pores) in a Chevron configuration produce pulses less than 1 ns wide, with rise times of less than 500 ps.

We have found that an accelerating voltage between the Chevron plates improves the rise times of the output pulses. Fig. 12 shows a sampling oscilloscope trace of Chevron pulses produced by single low energy positive ions; the Chevron plates had 12  $\mu\text{m}$  pores and a 200 V interplate accelerating voltage between them. The output signal was derived from a 50  $\Omega$  conical anode, connected directly to the input of the sampling oscilloscope. The anode was held at ground potential with the adjacent MCP electrode at  $-500$  V.

The Chevron and conical anode are shown in fig. 13. The coaxial design eliminates pulse reflection and subsequent "ringing" in the output pulse. The cones are precision machined to tight tolerances according to the formula<sup>49</sup>):

$$Z = 60 \ln (\cos \frac{1}{2}\alpha_1 / \cos \frac{1}{2}\alpha_2), \quad (6)$$

where  $\alpha_1$  is the semi-angle of the inner cone and  $\alpha_2$  the semi-angle of the outer cone. Both are mounted on a 50  $\Omega$  Genrad<sup>50</sup>) connector. After

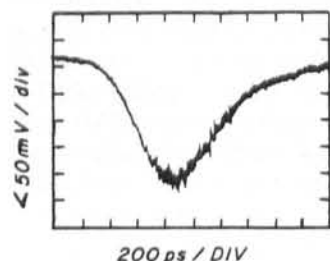


Fig. 12. Sampling oscilloscope trace of Chevron (200 V interplate bias) output pulses. Signal was derived from a 50  $\Omega$  conical anode.

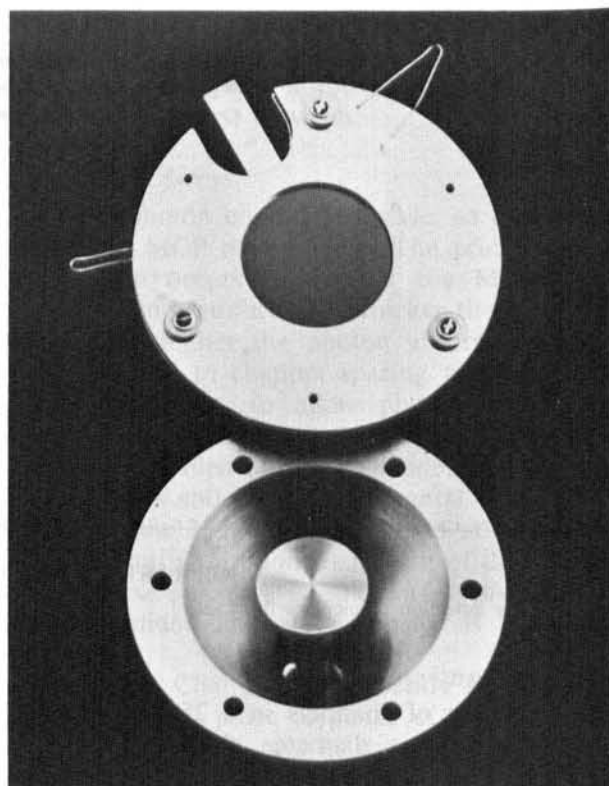


Fig. 13. Chevron and 50  $\Omega$  anode.

correction for the bandwidth of the measurement electronics, we found that the pulse rise time was reduced from 675 ps to 360 ps by application of a 200 V interplate bias voltage. In the latter case, the pulse fwhm was about 750 ps.

The time response of an LEP HR 350 MCP photomultiplier tube has recently been reported by Leskovar and Lo<sup>51</sup>). Such a device consists of a high gain curved channel (40  $\mu\text{m}$ ) MCP sandwiched between an S-20 photocathode and a 50  $\Omega$  anode. Using pulsed optical techniques, these authors measured a pulse rise time of 640 ps, and a single photoelectron time spread fwhm of  $< 200$  ps. The multiphotoelectron time spread was measured to be 160 ps and 56 ps for  $10^2$  and  $10^3$  photoelectrons per pulse respectively, in agreement with the expectation that the time resolution should be proportional to  $\sqrt{n_e}$ , where  $n_e$  is the number of primary incident electrons.

#### 4.4. MAGNETIC FIELD IMMUNITY

Because of the small dimensions and correspondingly high electric field strengths, it is expected that MCPs and particularly photomultiplier tubes

based on proximity focused MCPs should exhibit a high degree of immunity to magnetic fields. Lo et al.<sup>52)</sup> report satisfactory performance of the LEP HP 350 photomultiplier tube at axial magnetic fields up to 2 kG and transverse magnetic fields up to 700 G. The latter figure is 2–3 orders of magnitude improvement over conventionally designed photomultiplier tubes.

#### 4.5. DARK COUNT

Because of the relatively high work function of the lead glasses used in MCP, the thermal emission rates of electrons resulting in high gain output pulses are extremely low. Typically, at room temperature, the dark count from a Chevron is on the order of 1 count/cm<sup>2</sup> s. This is remarkable, considering the fact that a 25 mm diameter channel plate with 12  $\mu$ m pores has a true internal area of lead glass in contact with the vacuum environment of 380 cm<sup>2</sup>. Dark count does begin to increase at pressures higher than 10<sup>-6</sup> torr because of ion feedback effects.

#### 4.6. MCP LIFETIME

The lifetime of an MCP is determined by changes in the channel wall secondary emission coefficient due to electron scrubbing, especially in the high gain region of a channel. Consequently, the gain drops as a function of accumulated count.

Timothy and Bybee<sup>53)</sup> have measured the modal gain change as a function of accumulated count for a high gain Mullard J-plate (the channels are J-shaped with the high curvature at the output).

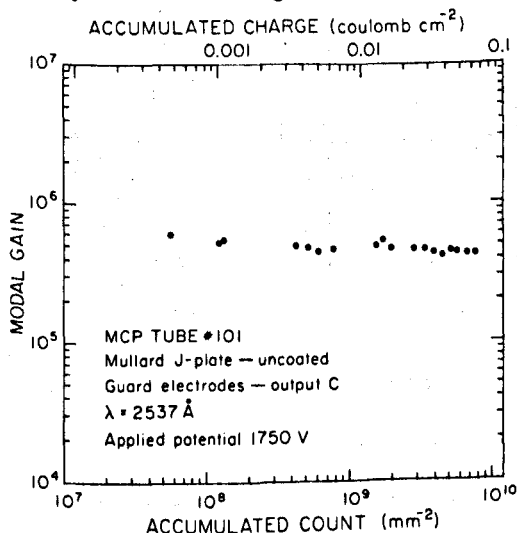


Fig. 14. Modal gain vs accumulated count for a curved channel MCP (from ref. 53).

The plate was mounted in a laboratory evaluation tube with a multianode read out. Referenced to a discriminator level of 10<sup>5</sup> electrons/pulse, they observed a loss of gain of only about 20% at an accumulated total of 2 × 10<sup>10</sup> counts/mm (see fig. 14). This is the kind of performance expected from previous experience with single channel multipliers, and is greatly superior to the performance reported by Sandel et al for straight channel MCPs<sup>54)</sup>.

#### 5. Applications

Microchannel plates were originally developed as high resolution electron amplification devices for image intensifiers. A schematic diagram of a proximity focused tube is shown in fig. 15. Typically, a 300 V potential maps the electron image from a photocathode onto the input of a straight channel MCP operated at a gain of 10<sup>3</sup>–10<sup>4</sup>. Output electrons are accelerated by 6 kV into a phosphor screen. The screen, usually of a P-20 or P-11 type for visual observation, is aluminized to prevent optical feedback to the photocathode, and to increase the light output to the observer. A P-47 phosphor, with an 80 ns decay time, is sometimes used for fast pulsed operation. Gating may be achieved by swinging the cathode potential 50 V positive with respect to the MCP input. Overall tube gain is the product of photocathode quantum efficiency, MCP gain, and the optical gain produced by the energetic electrons striking the phosphor.

High speed photomultipliers such as the LEP HR 350 substitute a high gain curved channel plate and a conical 50  $\Omega$  anode. The performance characteristics of these devices have been recently reviewed<sup>55)</sup>. Their speed and high level of immunity to stray magnetic fields makes their use in fast scintillation counting most attractive.

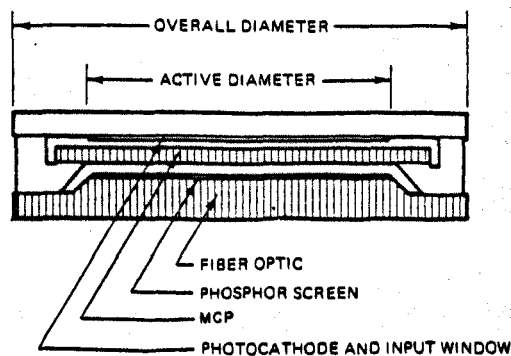


Fig. 15. A proximity focus image intensifier tube.

Other electronic tubes which utilize MCPs have been described by Pietri<sup>56</sup>). Of particular interest is the use of an MCP in proximity focus with the phosphor screen of a Cathode Ray Tube. This allows use of low beam currents and low acceleration potentials necessary for high writing speeds; the latter are concomitant with a high bandwidth ( $\sim$  several GHz) real time oscilloscope.

The use of MCPs for the direct detection of charged particles and energetic photons has resulted in the development of various methods for electronic recording of spatial information. Giffin et al.<sup>57</sup>) have developed a detector for use with a Mattauch-Herzog focal plane mass spectrometer, which consists of a linear mosaic of straight channel plates and a phosphor screen. A fiber optic image dissector folds the  $36\text{ cm} \times 0.5\text{ cm}$  focal plane image into the  $1.27\text{ cm} \times 1.27\text{ cm}$  format of a vidicon.

Methods of event localization which dispense with the phosphor screen are also available. Since the optical gain of the phosphor conversion is no longer available, such methods generally require high gain MCP configurations, i.e., a Chevron or curved channel MCP. An output pulse at  $10^7$  gain develops about 100 mV across a  $50\ \Omega$  load. One

obvious technique is to use a multi-anode scheme, whereby the MCP output charge is mapped by proximity focusing onto electrically independent conducting anode elements. This technique allows operation at high count rates since the sense elements all act in parallel, but at the cost of electronic complexity. A  $10 \times 10$  multi-anode matrix requires 100 pre-amplifier/amplifier/discriminators (PADs).

A simplification can be achieved by use of the coincidence anode of Timothy and Bybee<sup>53</sup>). Here the count rates from  $(n \times m)$  image elements are read out with a total of  $(n+m)$  PADs. The anode employs two sets of orthogonal linear anodes (row and column) and event location is determined by the coincidence of row and column pulses. Both a two-dimensional format ( $512 \times 512$  elements) and a folded one-dimensional format ( $2 \times 1024$  elements) have been fabricated.

MCP event location may also be determined by a resistive anode using charge division<sup>58-61</sup>) or rise time<sup>28</sup>) encoding techniques similar to those developed by Borkowski and Kopp<sup>62</sup>) for resistive wire proportional counters.

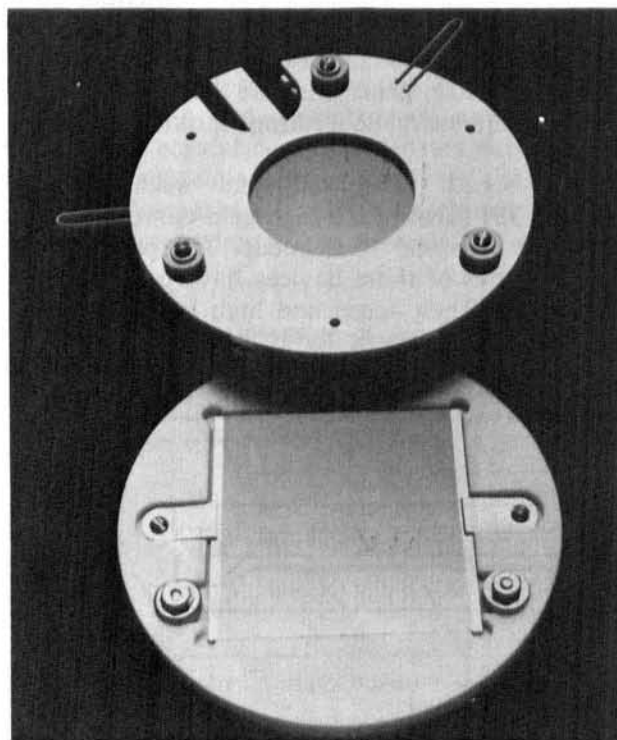


Fig. 16. A Chevron with resistive anode encoder (RAE).

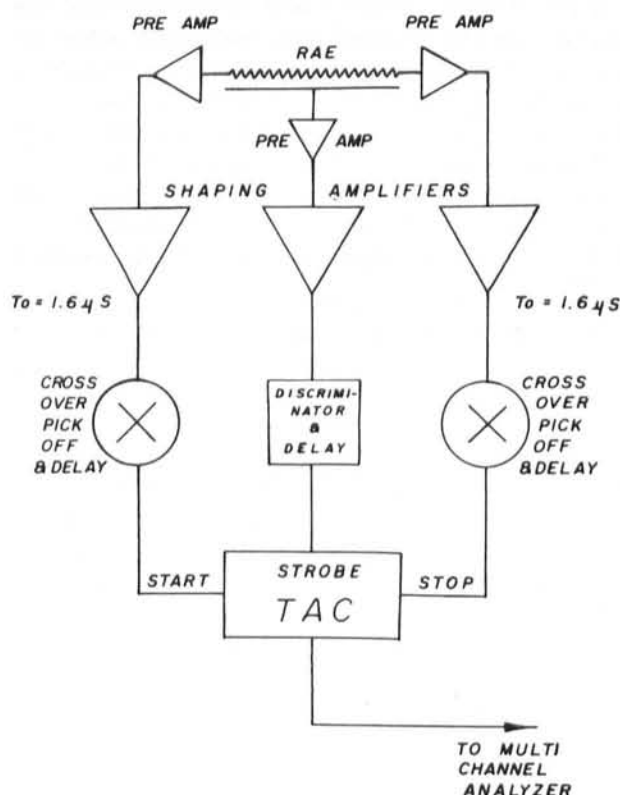


Fig. 17. Electronics block diagram for a one-dimensional RAE (rise time method).

The author has fabricated one-dimensional resistive anode encoders (RAE) for use with a 25 mm Chevron (see fig. 16). The resistive sheet is basically a thick film resistive glaze on a 38 mm  $\times$  38 mm ceramic substrate. Electrical contact is made with vacuum-deposited chromium electrodes at opposing edges of the sheet. A rear metal plate defines a parallel plate capacitance  $C_T \approx 28$  pF and the total sheet resistance  $R_T$  was chosen to be about 250 k $\Omega$ . The resistive anode was tested at a distance of several mm from the rear MCP, such a large separation being acceptable due to the centroid averaging property of the RAE. An accelerating potential of at least 150 V between Chevron and RAE was required to ensure optimum spatial resolution.

Performance testing was accomplished using the rise time method, and an electronic block diagram is shown in fig. 17. The technique utilizes the fact that the difference in pulse rise time at each end of the resistive strip, considered to be a diffusive RC line, is a measure of the position at which the pulse originates. After suitable bipolar shaping with time constant  $T_0$ , the rise time difference is translated to a difference in cross-over time, and a pair of cross-over pick-offs provide stop/start signals to a time to amplitude converter (TAC), the output of which is routed to a multi-channel analyzer. A delay in the "stop" arm of the system allows appropriate setting of position zero. A capacitively coupled signal is derived from the RAE back flange, and a resulting discriminator output is used to strobe the TAC, allowing a noise threshold to be set. All the electronics were commercially available NIM modules, and charge sensitive pre-amplifiers were used.

According to Mathieson<sup>63</sup>), optimum linearity and minimum spatial resolution should be obtained with  $T_0$ , the time constant of the bipolar shaping amplifiers, given by  $T_0 = 2R_TC_T/\pi^2$ , which in the present case turns out to be 1.6  $\mu$ s.

Tests were performed with a 100  $\mu$ m wide beam of 1216  $\text{\AA}$  U.V. radiation; integral non-linearity over the 25 mm diameter format was 0.3% and the spatial uncertainty was about 50  $\mu$ m. This latter figure was obtained at a Chevron gain of  $10^7$ , and is a linear function of the charge per pulse. Some broadening of the TAC output distribution was observed at random count rates in excess of 10 kHz, but the RAE performed reasonably out to 40 kHz.

The resistive anode encoder can also be used for

two-dimensional analysis<sup>59</sup>). The simplest method is to put electrodes at the four corners of the resistive sheet and to process  $x$  and  $y$  information independently. A coincidence requirement on the  $x$  and  $y$  TAC outputs then establishes a unique event location. This method suffers from some pincushion distortion for events occurring near the corners of the sheet.

For handling moderate count rates with good spatial resolution, the resistive anode allows a mechanical and electronic simplicity which should be attractive in many applications.

Several applications in nuclear science utilize the superior time resolution available when MCPs are used as electron detectors. Green et al.<sup>4</sup>) used a Chevron with a flat metal anode in a fast-slow coincidence system to measure the half-lives of excited states of  $^{182}\text{W}$  at 0.100 keV and 1289.1 keV. The Chevron detected beta particles and conversion electrons, while gamma rays were detected with a Ge(Li) detector; the system time resolution was better than 100 ps. Gabor et al.<sup>64</sup>) have used a Chevron for the detection of secondary electrons from thin Carbon foils in a relativistic heavy ion time of flight system. More recently, Back et al.<sup>65</sup>) have used a time of flight mass identification system for fusion cross section measurements of the  $^{16}\text{O} + ^{27}\text{Al}$  reaction. A start pulse was provided by a Chevron and thin carbon foil set at 45° to the direction of the scattered particles, the foil acting as a source of secondary electrons. A Si surface barrier, at the end of a 67 cm flight path supplied the stop pulse. The time and

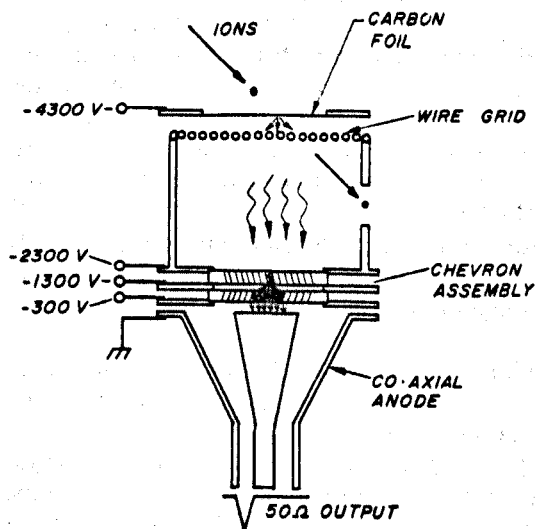


Fig. 18. A Chevron "start" detector (adapted from ref. 66).

energy resolution of this system were  $<150$  ps and 300 keV for 80 MeV  $^{16}\text{O}$  ions, respectively.

A carbon foil Chevron detector similar to that described by Goulding and Harvey<sup>66)</sup> is shown in fig. 18. The Chevron is operated at 1 kV/plate with no interplate bias voltage. A grid, 2 kV positive with respect to the carbon foil, and in close proximity to the foil is used to equalize the transit times of secondary electrons emitted at various angles. Girard and Bolore<sup>5)</sup> have determined the time resolution of a similar system to be 62 ps for fission fragments and 84 ps for  $\alpha$ -particles from a  $^{252}\text{Cf}$  source. They used a conical 50  $\Omega$  anode directly into an Ortec 473 Constant Fraction Discriminator. Finally, Zebelman et al.<sup>67)</sup> have developed a zero time detector using a magnetic field to provide the isochronous transport of secondary electrons from a carbon foil to a Chevron. These authors measured a time of flight resolution between this timing detector and a 120  $\mu\text{m}$  silicon detector of 90 ps and 150 ps for 104 MeV  $^{16}\text{O}$  ions and 8.78 MeV alpha particles, respectively.

## 6. Future developments

Summarized below are but a few of the developments in MCP technology which are under active investigation at this time:

1) Thick (5–10 mm) channel plates for enhanced efficiency in gamma-ray imaging applications. Galileo has fabricated such plates with efficiencies of 25% at energies just below the K absorption edge of lead at 88 keV. The plates are capable of space charge saturation, and have been tested as the front element in a Chevron.

2) Funneling of the input channels. This increases the open area ratio from 55% to 90% and allows a proportional increase in electron collection efficiencies when thin films are used over the input electrode of the MCP. The latter are used to suppress positive ion feedback to highly sensitive photocathodes.

3) High strip current MCPs. This of course allows operation at even higher count rates because of the concomitant reduction in channel recovery time.

4) MCPs with channel diameters of 8  $\mu\text{m}$  or less. Such plates will be capable of higher spatial and temporal resolution.

Finally, it is worth noting that MCPs can be fabricated in a wide range of geometric formats, both circular and rectangular. 127 mm diameter MCPs have been "slumped" to a spherical curve,

and annular MCPs have been made to encompass an accelerator beam. The possibilities for such variations are virtually limitless.

The author wishes to thank F. Baker for help with the figures. He also wishes to thank G. Timothy of Harvard College Observatory and J. Chang of Sandia Laboratories for permission to reproduce fig. 14 and 11, respectively, from their published work.

## References

- 1) E. Kellogg, P. Henry, S. Murray and L. Van Speybroeck, *Rev. Sci. Instr.* **47** (1976) 282.
- 2) M. Lampton, W. Cash, R. F. Malina and S. Bowyer, *X-ray imaging*, Proc. SPIE **106**, (1977) p. 93.
- 3) K. W. Dolan and J. Chang, *ibid.*, p. 178.
- 4) M. I. Green, P. F. Kenealy and G. B. Beard, *Nucl. Instr. and Meth.* **126** (1975) 175.
- 5) J. Girard and M. Bolore, *Nucl. Nucl. Instr. and Meth.* **140** (1977) 279.
- 6) J. P. Boutot, J. C. Delmotte, J. A. Mieké and B. Sipp, *Rev. Sci. Instr.* **48** (1977) 1405.
- 7) P. T. Farnsworth, *Electron Multiplier*, U.S. Patent N. 1, 969, 399 (1930).
- 8) P. K. Oschepkov, B. N. Skvortsov, B. A. Osanov and I. V. Siprikov, *Pribory. Tekh. Eksper.* **4** (1960) 89.
- 9) G. W. Goodrich and W. C. Wiley, *Rev. Sci. Instr.* **33** (1962) 761.
- 10) J. Adams and B. W. Manley, *Electron Eng.* **37** (1965) 180.
- 11) J. Adams and B. W. Manley, *IEEE Trans. Nucl. Sci.* **NS-13** (1966) 88.
- 12) H. Bruining, *Physics and applications of secondary electron emission* (Pergamon Press, London, 1954).
- 13) R. L. Green and K. B. Blodgett, *J. Am. Ceramic Soc.* **31** (1948) 89.
- 14) D. Washington, V. Duchenois, R. Polaert and R. M. Beasley, *Acta Electronica* **14** (1971) 201.
- 15) W. C. Wiley and C. F. Hendee, *IRE Trans. Nucl. Sci.* **NS-9** (1962) 103.
- 16) G. Eschard and B. W. Manley, *Acta Electronica* **14** (1971) 19.
- 17) P. Schagen, *Advances in image pick-up and display*, vol. 1 (Academic Press, New York, 1974) p. 1.
- 18) A. J. Guest, *Acta Electronica* **14** (1971) 79.
- 19) D. S. Evans, *Rev. Sci. Instr.* **36** (1965) 375.
- 20) K. C. Schmidt and C. F. Hendee, *IEEE Trans. Nucl. Sci.* **NS-13** (1966) 100.
- 21) T. A. Somer and P. Graves, *IEEE Trans. Nucl. Sci.* **NS-16** (1969) 376.
- 22) C. Loty, *Acta Electronica* **14** (1971) 107.
- 23) J. G. Timothy and R. L. Bybee, *Rev. Sci. Instr.* **48** (1977) 202.
- 24) P. Henkel, R. Roy and J. L. Wiza, *IEEE Trans. Nucl. Sci.* **NS-25** (1978) 548.
- 25) V. Chalmerton and P. Chevalier, *Acta Electronica* **14** (1971) 99.
- 26) W. B. Colson, J. McPherson and F. T. King, *Rev. Sci. Instr.* **44** (1973) 1694.

- 27) J. L. Wiza, P. R. Henkel and R. L. Roy, *Rev. Sci. Instr.* **48** (1977) 1217.
- 28) W. Parkes, K. D. Evans and E. Mathieson, *Nucl. Instr. and Meth.* **121** (1974) 151.
- 29) J. P. Boutot, G. Eschard, R. Polaert and V. Duchenois, *Proc. 6th Symp. on Photo-electronic image devices*, London, (1974), publ. in *Advan. Electron. Electronic Phys.*, **40A** (1976) 103.
- 30) LEP - Laboratoires d'Electronique et de Physique Appliquée, Limeil Brevannes, France.
- 31) Mullard Ltd., Torrington Place, London WC1, England.
- 32) J. G. Timothy, *Rev. Sci. Instr.* **45** (1974) 834.
- 33) J. G. Timothy and R. L. Bybee, *Proc. SPIE Int. Techn. Symp.*, San Diego, California (August, 1977).
- 34) H. J. S. Trapp, *Acta Electronica* **14** (1971) 41.
- 35) J. P. Macau, J. Jamar and S. Gardier, *IEEE Trans. Nucl. Sci.* **NS-23** (1976) 2049.
- 36) G. E. Hill, *Proc. 6th Symp. on Photo-electronic image devices*, London (1974), publ. in *Advan. Electron. Electronic Phys.* **40A** (1976) 153.
- 37) M. Galanti, R. Gott and J. F. Renaud, *Rev. Sci. Instr.* **42** (1971) 1818.
- 38) B. Tatry, J. M. Bosqued and H. Reme, *Nucl. Instr. and Meth.* **69** (1969) 254.
- 39) F. Paresce, *Appl. Optics* **14** (1975) 2823.
- 40) D. G. Smith and K. A. Pounds, *IEEE Trans. Nucl. Sci.* **NS-15** (1968) 541.
- 41) P. J. Bjorkholm, L. P. Van Speybroeck and M. Hecht, *X-ray imaging*, *Proc. SPIE* **106** (1977) p. 189.
- 42) S. Siddiqui, *J. Appl. Phys.* **48** (1977) 3053.
- 43) J. P. Henry, E. M. Kellogg, U. G. Briel, S. S. Murray, L. P. Van Speybroeck and P. J. Bjorkholm, *X-ray imaging*, *Proc. SPIE* **106** (1977) p. 196.
- 44) A. P. Lukirskii, E. P. Savinov, I. A. Brytov and Yu. F. Shepelev, *USSR Acad. Sci. Bull. Phys.* **28** (1964) 774.
- 45) Corning 8161 Glass, U.S. Patent 2, 964, 414.
- 46) W. Parkes, R. Gott and K. A. Pounds, *IEEE Trans. Nucl. Sci.* **NS-17** (1970) 360.
- 47) J. Adams and I. C. P. Millar, *Acta Electronica* **14** (1971) 237.
- 48) A. Seko and H. Kobayashi, *Rev. Sci. Instr.* **44** (1973) 400.
- 49) G. Beck, *Rev. Sci. Instr.* **47** (1976) 849.
- 50) GenRad Corp., Concord, Mass., U.S.A.
- 51) B. Lescovar and C. C. Lo, *IEEE Trans. Nucl. Sci.* **NS-25** (1978) 582.
- 52) C. C. Lo, P. Lecomte and B. Lescovar, *IEEE Trans. Nucl. Sci.* **NS-24** (1977) 302.
- 53) J. G. Timothy and R. L. Bybee, *Proc. SPIE Int. Techn. Symp.*, San Diego, California (August, 1977).
- 54) B. R. Sandel, A. L. Broadfoot and D. E. Shemansky, *Appl. Optics* **16** (1976) 1435.
- 55) S. Dhawan and R. Majka, *IEEE Trans. Nucl. Sci.* **NS-24** (1977) 270.
- 56) G. Pietri, *IEEE Trans. Nucl. Sci.* **NS-24** (1977) 228.
- 57) C. E. Giffin, H. G. Boettger and D. D. Norris, *Int. J. Mass Spectrom. Ion Phys.* **15** (1974) 437.
- 58) C. D. Moak, S. Datz, F. Garcia Sanlebané and T. A. Carlson, *J. Electron Spectroscopy and Related Phenomena* **6** (1975) 151.
- 59) M. Lampton and F. Paresce, *Rev. Sci. Instr.* **45** (1974) 1098.
- 60) G. M. Lawrence and E. J. Stone, *Rev. Sci. Instr.* **46** (1975) 432.
- 61) H. Weiser, R. C. Vitz, H. W. Moos and A. Weinstein, *Appl. Optics* **15** (1976) 3123.
- 62) C. J. Borkowski and M. K. Kopp, *Rev. Sci. Instr.* **46** (1975) 951.
- 63) E. Mathieson, *Nucl. Instr. and Meth.* **97** (1971) 171.
- 64) G. Gabor, W. Schimmerling, D. Greiner, F. Bieser and P. Lindstrom, *Nucl. Instr. and Meth.* **130** (1975) 65.
- 65) B. B. Back, R. R. Betts, C. Gaarde, J. S. Larsen, E. Michelsen and Tai Kuang-Hsi, *Nucl. Phys.* **A285** (1977) 317.
- 66) F. S. Goulding and B. G. Harvey, *Ann. Rev. Nucl. Sci.* **25** (1975) 203.
- 67) A. M. Zebelman, W. G. Meyer, K. Halback, A. M. Poskanzer, R. G. Sextro, G. Gabor and D. A. Landis, *Nucl. Instr. and Meth.* **141** (1977) 439.